The Relationship between Oscillating Subtropical Wind Stress and Equatorial Temperature*

BARRY A. KLINGER+

Oceanographic Center, Nova Southeastern University, Dania Beach, Florida

JULIAN P. MCCREARY JR.

International Pacific Research Center, University of Hawaii, Honolulu, Hawaii

RICHARD KLEEMAN

Courant Institute for Mathematical Sciences, New York University, New York, New York

(Manuscript received 27 October 2000, in final form 18 September 2001)

ABSTRACT

An earlier study showed that an atmosphere–ocean model of the Pacific develops a midlatitude oscillation that produces decadal sea surface temperature (SST) variability on the equator. The authors use the ocean component of this model to understand better how subtropical wind stress oscillations can cause such SST variability. The model ocean consists of three active layers that correspond to the mixed layer, the thermocline, and intermediate water, all lying above a motionless abyss.

For a steady wind, the model develops a subtropical cell (STC) in which northward surface Ekman transport subducts, flows equatorward within the thermocline, and returns to the surface at the equator. Analytic results predict the model's equatorial temperature, given some knowledge of the circulation and external forcing. A prescribed subtropical wind stress anomaly perturbs the strength of the STC, which in turn modifies equatorial upwelling and equatorial SST.

The transient response to a switched-on wind perturbation is used to predict the ocean response to an oscillating wind. This method correctly predicts the results of several numerical experiments, and extends these results to a wide range of forcing periods. For an oscillating wind, there is a more complicated relationship between perturbations to equatorial SST and the various branches of the STC. The thermocline-branch anomalies are generally weaker than those in the surface and equatorial-upwelling branches. Equatorial SST anomalies lead, follow, and are roughly coincident with, variations in the thermocline, surface, and upwelling branches, respectively. Thus, while recent studies have suggested using the subsurface branch variations as a predictor of tropical–subtropical interactions, the surface branch may be a better predictor.

1. Introduction

A coupled ocean–atmosphere model of the Pacific Ocean has demonstrated a mode in which midlatitude dynamics may remotely force variations in equatorial sea surface temperature (SST: Kleeman et al. 1999, henceforth KMK). In the model, feedback between SST, wind, and heat flux in the subtropics and midlatitudes produces an oscillation in the wind stress. The wind stress oscillation, in turn, affects the meridional overturning circulation, known as the subtropical cell (STC), in which poleward subtropical Ekman transport subducts at midlatitudes, flows toward the equator within the thermocline, upwells in the eastern equatorial ocean, and returns to midlatitudes in the surface layer. A strengthening of the STC, then, increases the amount of thermocline water that upwells in the equatorial region, and so lowers equatorial SST below what it would be if it were completely controlled by local surface boundary conditions. Decadal oscillations in the strength of the STC therefore produce decadal oscillations in equatorial SST. In this study, we explore how surface wind stress, particularly in the subtropics, influences the strength of the STC and hence of equatorial temperature variations.

Throughout this paper, we use the term ''equatorial

* School of Ocean and Earth Science and Technology Contribution Number 5893, and International Pacific Research Center Contribution Number 122.

+ Current affiliations: George Mason University, Fairfax, Virginia, and Center for Ocean–Land–Atmosphere Studies, Calverton, Maryland.

Corresponding author address: Dr. Barry A. Klinger, Center for Ocean–Land–Atmosphere Studies, Calverton, MD 20705.
E-mail: klinger@cola.iges.org

upwelling'' to refer only to the part of the total upwelling field that participates in the STC, that is, the part associated with a transfer of relatively cool thermocline water into the surface layer. We ignore the upwelling that is associated with the shallower tropical and equatorial cells (McCreary and Lu 1994; Lu et al. 1998, section 2), which are closed by downward mixing of surface water within the Tropics, and so are not as thermodynamically significant. It should be emphasized, however, that the *total* amount of equatorial upwelling (that is, the sum of contributions from the subtropical, tropical, and equatorial cells) is determined by the equatorial winds, not by STC strength.

KMK considered the coupled system, but the ocean component by itself presents many questions. Since variations in STC strength seem to be driving equatorial temperature variations in the KMK solutions, it is interesting to consider how equatorial temperature is affected by upwelling strength. On an elementary level, we know that the equatorial cold tongue exists because of the upwelling of cold water, but how does the temperature depend on upwelling strength and other key parameters?

It is also of fundamental interest to understand how oscillatory solutions differ from steady ones. Presumably, if the forcing varies slowly enough, the circulation will always be close to equilibrium, and flow patterns and dynamics will be close to the steady behavior explored by McCreary and Lu (1994), Liu (1994), Liu et al. (1994), Liu and Philander (1995), Lu and McCreary (1995), Rothstein et al. (1998), and Lu et al. (1998). In the steady state, STC strength is largely controlled by the zonal wind stress integrated along the edge of the Tropics, which changes the Ekman transport there; this change in the surface STC branch is balanced by equatorial upwelling and an opposite change in the subsurface circulation (McCreary and Lu 1994). For sufficiently fast evolution, transients could be significant, so the different branches of the STC circulation no longer change at the same rate (i.e., in a quasi-steady manner). The primary nature of this adjustment is important both from a conceptual and observational point of view, especially since recently much attention has focused on the lower branch, that is, on how thermocline water travels to the equator (Deser et al. 1996; Gu and Philander 1997; Zhang et al. 1998). While it is natural to look upstream for the source of equatorial SST variations, it may be necessary to look at all STC branches in order to understand how changes propagate.

The wind perturbations generated by KMK's coupled model had a rich spatial structure, with especially strong amplitudes north of 40°N. Inui et al. (1999) looked at the response to a perturbation to midlatitude wind, but did not focus on the STC. While the steady STC is hardly affected by winds poleward of the subtropics (McCreary and Lu 1994), there may be a greater effect in the transient case. Therefore it is interesting to see if the oscillating case enhances the importance of midlatitude wind-stress anomalies, and more generally whether the details of geometrically complicated wind patterns are more important to the oscillating response than they are to the steady response.

We address the issues raised here through a series of numerical experiments using a version of the ocean component of KMK's coupled model. The numerical model is simple enough to analyze relatively easily, computationally inexpensive enough to carry out a large number of experiments on a desk-top workstation, yet realistic enough to reproduce the main features of the surface, thermocline, and intermediate water circulation of the Pacific. We conduct a ''Base Run'' with climatological surface forcing, as well as a series of experiments with steady and oscillating wind perturbations. The Base Run not only provides a standard of comparison for the perturbation experiments but also a testbed for ideas about equatorial SST. In particular, we introduce a simple analytic model of the surface temperature and test it against the Base Run. The perturbation experiments include zonal wind anomalies in various latitude bands as well as wind anomalies based on KMK's coupled results. We show that for forcing on decadal timescales, there are significant departures from the equilibrium response to steady perturbations. We then use the transient response to a steady perturbation to help understand the oscillating behavior.

2. The model

Our numerical model is based on the ocean model described in Lu et al. (1998) and used by KMK. It consists of three active layers with thicknesses h_i (i = 1, 3 is a layer index), temperatures T_i, and horizontal velocities $\mathbf{v}_i = (u_i, v_i)$, over a quiescent abyss. Flow between layer i and layer $i + 1$ is given by w_i, which can differ from the vertical velocity in regions where the layer interface is not horizontal. The active layers can be thought of as the region above the thermocline (layer 1), a thermocline layer (layer 2), and an intermediate or lower thermocline layer (layer 3). Because temperature can vary horizontally within a layer (salinity is ignored in this model), the layers do not have uniform density. This formulation allows us to maintain a relatively simple vertical structure that permits a subtropical cell, and allows us to study thermodynamic effects.

The model differs from that of Lu et al. (1998) in allowing temperature to vary over latitude, longitude and time within each layer. The evolution of T_i is governed by a discretized version of

$$T_{it} + \mathbf{v}_i \cdot \nabla T_i = \delta_{i1}\frac{H_q}{t_q h_1}(T_* - T_1) + C + [\kappa_2\nabla^2 T_i - \kappa_4\nabla^4 T_i] + \frac{1}{h_1}[w_i^+(T_{i+1} - T_i) + w_{i-1}^-(T_{i-1} - T_i)], \quad (1)$$

where δ_{i1} is the Kronecker delta symbol, T_* is a reference temperature to restore T_1, $H_q = 100$ m and $t_q = 180$ days control the strength of restoring, C represents the effect of a convective adjustment scheme which homogenizes statically unstable regions (McCreary and Lu 1994), $w_i^+ = \max(w_i, 0)$, $w_i^- = \min(w_i, 0)$, and $w_0 = 0$.

The model domain is a simplified version of the Pacific Ocean between 35°S and 55°N. In addition to the wind and surface temperature forcing described below, the model ocean is driven by inflow–outflow conditions designed to mimic exchange with the Southern Ocean and Indian Ocean; we refer to the circulation driven by this exchange as the Pacific interocean circulation (IOC). To represent the inflow of cold water from south of 35°S, 10 Sv (Sv $\equiv 10^6$ m^3 s^{-1}) of water enters layer 3 across the western boundary between 30° and 35°S. The model represents the Indonesian Throughflow with a port in the western boundary between 2°N and 6°N through which 5 Sv exits in each of the top two layers.

The experiments have grid resolution of 1° in latitude and 2° in longitude. Laplacian and biharmonic lateral dissipation are applied to both momentum (ν) and temperature (κ). Denoting Laplacian and biharmonic coefficients with subscripts 2 and 4, respectively, we use $\nu_2 = 10^5$ m^2 s^{-1}, $\kappa_2 = 0.5 \times 10^4$ m^2 s^{-1}, and $\nu_4 = \kappa_4 = 10^{14}$ m^4 s^{-1}. There is also a Laplacian layer-thickness diffusivity of 250 m^2 s^{-1}. The time step is 1/20 of a day, with a smoothing time step (for numerical purposes) performed every 41 time steps.

The parameterizations of subduction from, and entrainment into, the mixed layer is the same as in Lu et al. (1998), in which h_1 is restored towards $H_e = 50$ m with a time constant of $t_e = 1$ day and subduction is allowed to occur only poleward of $\pm y_d$, where $y_d = 23°$. In the Lu et al. (1998) $3\frac{1}{2}$-layer Pacific model, vertical mixing was parameterized by discretizing the vertical diffusion operator $\kappa_V \partial^2 T/\partial z^2$ so that the flow into layer 2 from the adjacent layers was based on the relative thickness of the three layers. In practice, this produced very little interlayer flow except in small regions where other dynamics of the system made h_2 small. Here, we take advantage of that behavior by simplifying the parameterization: Mixing only produces flow into layer 2 in regions where the layer thickness h_2 is less than $h_{2\min} = 20$ m, the across-interface flow is then exactly what is needed to restore h_2 to $h_{2\min}$, and we arbitrarily force equal amounts to flow into layer 2 from layers 1 and 3. The choices that we describe here are not critical because the results of Lu et al. (1998) indicate that the behavior of the subtropical cell is not very sensitive to the details of the mixing parameterization.

While internal dynamics set the depth of each layer, the total volume of the top three layers is constant because there is no mass exchanged with the abyssal layer. The mean depth of the top three layers is set to 750 m. Rather than restoring to the observed two-dimensional SST field of the ocean, T_1 is restored to a zonally uniform profile $T_*(y)$ in order to allow the internal dynamics of the model (notably equatorial upwelling and western boundary currents) to produce zonal temperature structure. The reference profile is taken from annual-average climatology (Levitus and Boyer 1994) at longitude 175°W, a region of the ocean that has relatively weak horizontal currents and upwelling. To prevent numerical problems that develop in regions where T_* is extremely cold, we set values of T_* colder than 10°C to 10°C. The abyssal layer temperature is set to 5°C. The initial value of T_3 is 8°C, and it stays within 0.006°C of this value throughout the integrations because T_3 is controlled by the inflow which is also set to 8°C.

The numerical experiments consist of a Base Run, driven by smoothed, annual-average wind stress fields of Hellerman and Rosenstein (1983) shown in Fig. 1a. The amplitude of the wind stress is multiplied by a factor of 0.7 because this dataset is believed to be too strong in the Tropics (Harrison 1989). Other experiments are driven by various perturbations to this forcing as discussed next.

According to McCreary and Lu (1994) and Lu et al. (1998), STC strength is primarily set by the zonally integrated Ekman transport at the subduction latitudes $\pm y_d$. To explore this idea, we conduct experiments that are identical to the Base Run except that zonally uniform, zonal wind stress anomalies are added to the climatological wind field. The wind perturbations in these ''simple wind'' experiments are given by

$$\tau' = \frac{1}{2} a_0 \left[1 - \cos\left(2\pi \frac{y - y_{\min}}{y_{\max} - y_{\min}} \right) \right], \qquad (2)$$

where A_0 is the amplitude of the perturbation, y is latitude, and $y_{\min}$ and $y_{\max}$ are the latitude boundaries of the perturbation. Meridional profiles of the perturbations and total winds are shown in Figs. 1b,d. In all experiments, $|a_0| = 0.125$ dyn cm^{-2}. In two experiments, we use a perturbation between 7° and 39°N (easterlies in the ''Strong Trades'' run and westerlies in the ''Weak Trades'' run). The ''Weak Westerlies'' experiment has an easterly perturbation between 23° and 55°N. Because the strength of the STC is largely set by the Ekman transport at y_d (McCreary and Lu 1994), the last experiment should have little or no effect on tropical temperature.

Another experiment is performed with wind perturbation based on the SVD3 pattern of KMK (Fig. 1c). The SVD3 pattern represents one of the joint modes of variability in wind stress and SST in the real world. In KMK's study it is associated with decadal variability, and hence is of particular interest for understanding how the ocean might respond to typical decadal wind changes. The amplitude used here has about the same zonally averaged zonal stress near y_d as the Strong Trades experiment does. As in KMK, for $|y_d| \leq y_d$, the wind stress is multiplied by a coefficient,

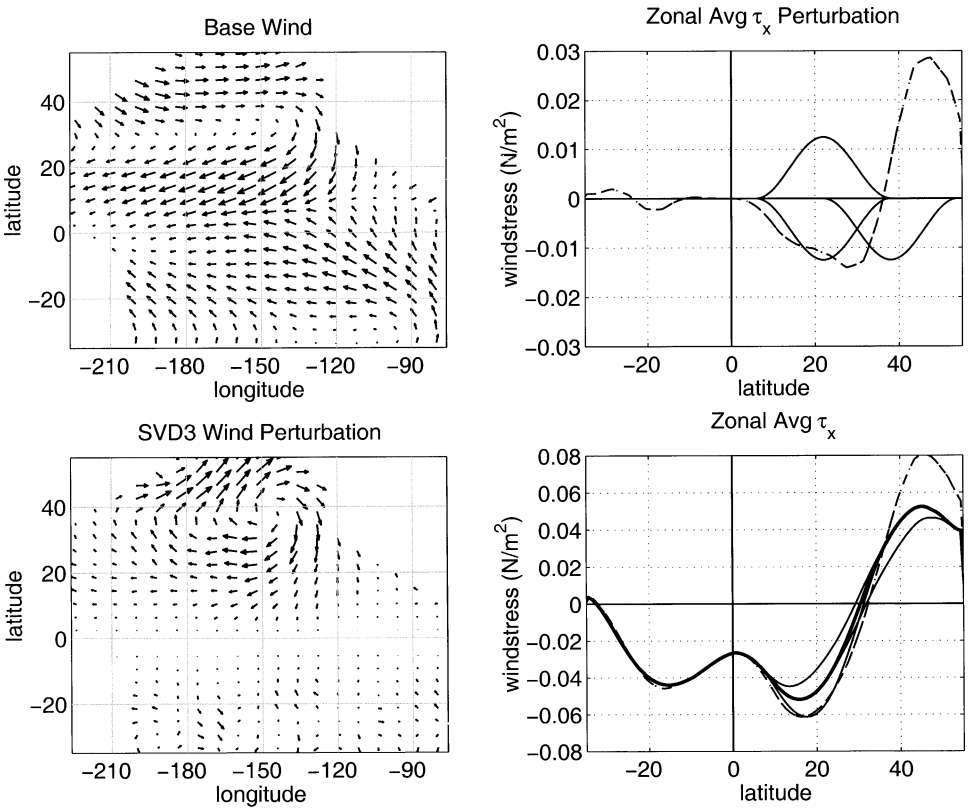

FIG. 1. Wind stress fields: (a) wind stress vectors for entire domain, Base Run; (b) zonal average of zonal wind stress perturbation, for simple wind profiles (solid lines) and SVD3 profile (dashed line); (c) SVD3 wind stress vectors; and (d) zonal average wind stress, line styles as in (b), thick line for Base Run. In (a) and (c), not every vector is shown.

$$c(y) = \frac{1}{2}\left[1 + \cos\left(2\pi\frac{|y| - y_d}{2y_d}\right)\right], \qquad (3)$$

which ranges from a value of 1 poleward of y_d to 0 at the equator. The equatorial truncation ensures that effects due to extratropical forcing are not contaminated by those caused by equatorial forcing. The resulting zonal-average perturbation is similar to the sum of the Strong Trades perturbation and a Strong Westerlies perturbation (Figs. 1b,d). To further identify the differences between simple wind patterns and the SVD3 pattern, an additional experiment, the ''Zonal SVD3'' experiment, has a zonally uniform zonal wind stress perturbation with the same zonal average as the SVD3 case.

We refer to the above perturbation experiments as ''switched-on'' experiments. ''Oscillating'' experiments use wind perturbations with the spatial patterns described above, but with amplitudes that vary sinusoidally in time according to

$$a(t) = a_0 \sin\left(2\pi\frac{t}{t_p}\right), \qquad (4)$$

where t_p is the forcing period. For the trades and SVD3 patterns, t_p is set to 12 and 24 yr; for the westerlies perturbation it is set to 12 yr only. Two different periods are used in order to obtain some information on how the response depends on the forcing period t_p.

3. Steady forcing

a. Base Run

The velocity field of the Base Run is similar to that of Lu et al. (1998). The top layer has a strong Ekman transport component of poleward flow in the subtropics, and the westward equatorial jet of the South Equatorial Current [Fig. 2a; for tropical surface observations see for example Johnson (2001)]. Layer 2, dominated by the subtropical gyre, has equatorward (and westward) flow in the subtropics feeding an eastward flowing Equatorial Undercurrent (Fig. 2b). Temperature T_1 is dominated by the meridional gradient imposed by the surface forcing, while T_2 has smaller variations (Figs. 2a,b).

The T_1 field is very close to $T_*(y)$ except in the midlatitude western-boundary currents and in the strong upwelling of the eastern equatorial region (Fig. 2a). If the ocean were motionless, T_1 would be identical to T_*. The question of how upwelling affects the equatorial tem-

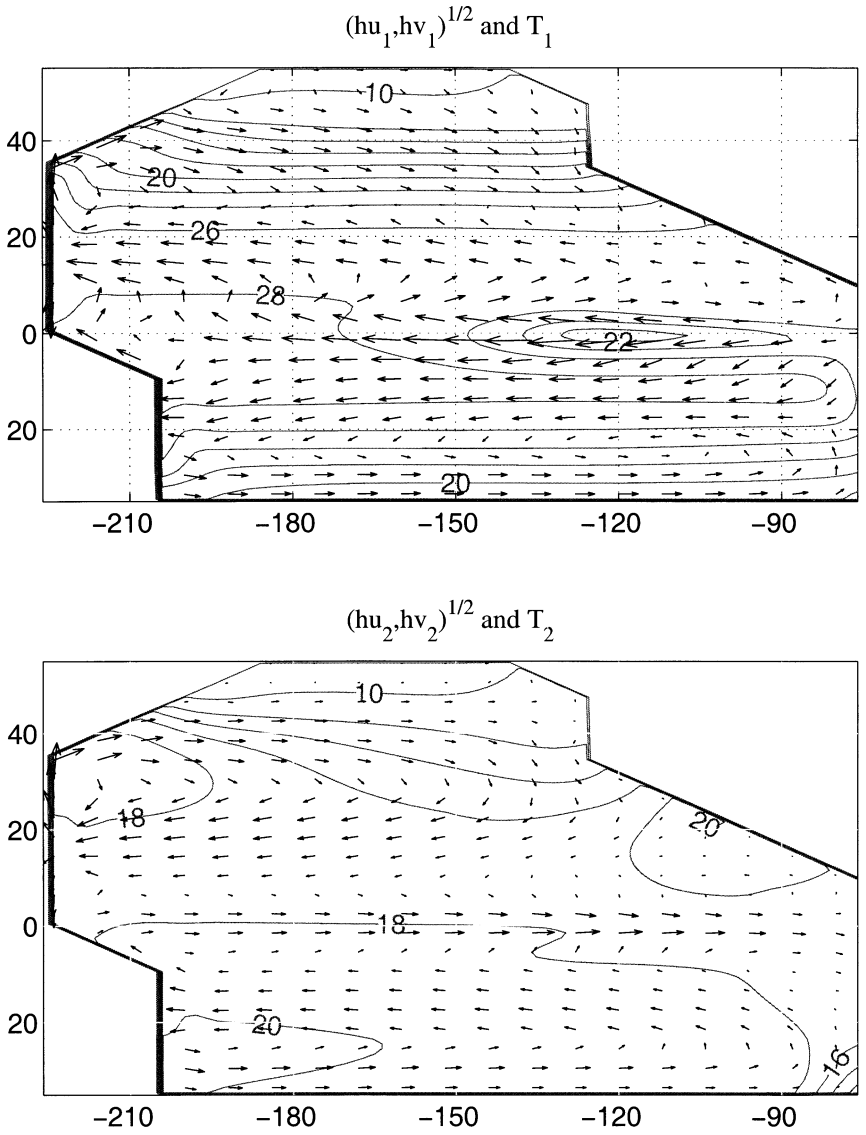

FIG. 2. General circulation for Base Run: (a) layer 1 vertical integral of horizontal velocity (arrows) and T_1; (b) same as (a) but for layer 2. For all panels, velocity is not shown at every grid point, lengths of arrows are proportional to the square root of vector magnitudes, and temperature contour intervals are 2°C.

perature $T_1(x, 0)$ can be rephrased as how much does the upwelling drag T_1 away from T_* toward T_2. Therefore it is convenient to define a nondimensional temperature perturbation

$$\theta = \frac{T_* - T_1}{T_* - T_2}. \tag{5}$$

If the temperature restoring is much stronger than upwelling, than the maximum value of θ found on the equator approaches 0, and if it is much weaker, the maximum value approaches $\theta = 1$.

Equatorial T_1 is nearly identical to T_* west of the dateline (Figs. 3a,b). East of about 130°W it is several degrees colder due to the upwelling there (Fig. 3c). There is a transition region in between where cool surface water is warmed to the restoring temperature as it flows westward. Along the equator, θ is greater than 0.4 over the eastern half of the basin (Fig. 3b), which indicates how strong an influence upwelled layer-2 water has. We will further discuss the steady equatorial T_1 in section 5.

b. Perturbation experiments

Having examined the Base Run we now proceed to the final (steady) states of the perturbation experiments. Key indices of the flow are W_{eq}, the upwelling volume transport from layer 2 to layer 1 integrated across the

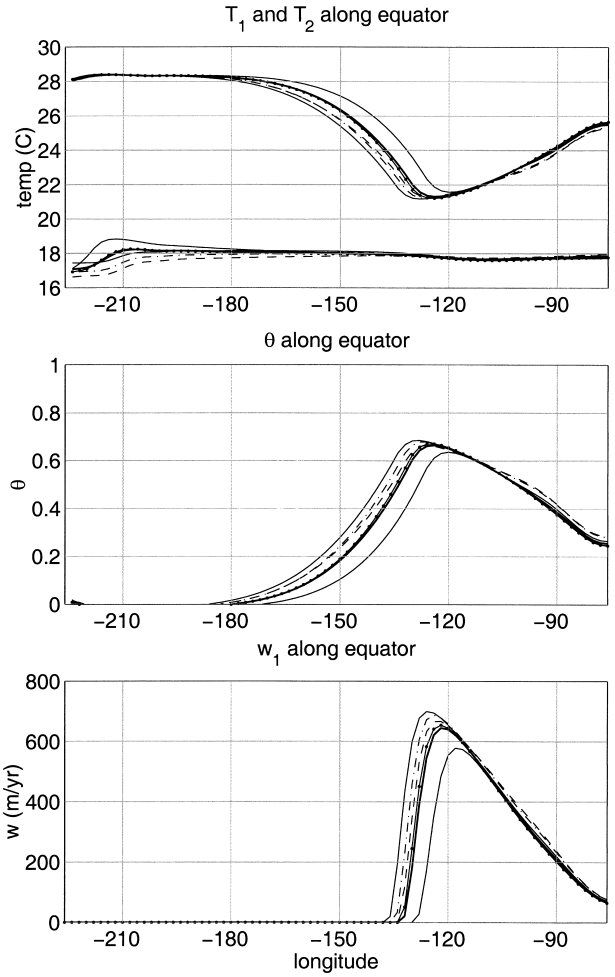

FIG. 3. (a) Plot of T_1 and T_2 as a function of x averaged from 0.5°N to 0.5°S. (b) θ for data in (a) using the average value of T_* in the region, 28.21°C. (c) Vertical velocity w_1 as a function of longitude along the equator, averaged as in (a). In all plots, thick line is Base Run, thin solid lines are trades perturbations (Strong Trades with colder T_1 and stronger w_1 than Base Run, Weak Trades the opposite), line with dots is Weak Westerlies, dashed line is SVD3, and dash–dot line is Zonal SVD3.

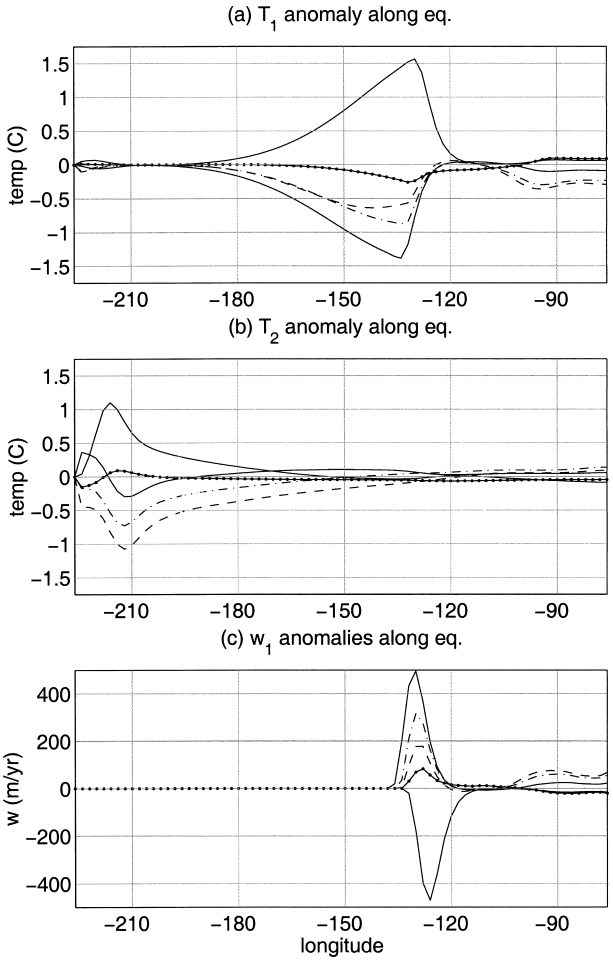

FIG. 4. Anomalies (relative to Base Run) of (a) T_1, (b) T_2, and (c) w_1 as a function of x, averaged from 0.5°S to 0.5°N. Trades experiments represented by plain solid lines, SVD3 by dashed line, Zonal SVD3 by dash–dot line, and Weak Westerlies by line with dots.

basin and from 5°S to 5°N, T_{eq} and θ_{eq}, the values of T_1 and θ averaged across the basin and from 0.5°S to 0.5°N, and $E(y)$ and $M_i(y)$, the meridional Ekman and layer volume transports integrated across the basin along latitude y. We focus on E and M_i at the edges of the Tropics, $\pm y_d$, and on the transport divergences, $\Delta M_i = M_i(y_d) - M_i(-y_d)$ and $\Delta E = E(y_d) - E(-y_d)$. In the Strong Trades, Weak Trades, and SVD3 experiments, there is about a 3 Sv anomaly in ΔE and ΔM_1, and the ΔM_2 anomaly is about 2 Sv. As expected from the results of McCreary and Lu (1994), the Weak Westerlies case has hardly any volume transport anomalies at the edges of the Tropics.

There are differences of 0.7 Sv between the magnitudes of the ΔM_1 and ΔM_2 anomalies. They are related to Ekman-pumping-induced changes in the thermocline thickness, $h_1 + h_2$ (Liu 1999), which produces changes in the net meridional flow in the upper two layers and compensating changes in layer 3. Upwelling associated with the IOC (defined in section 2) occurs in the Tropics and near the northern boundary. The wind anomalies change the proportion of upwelling in each region. The sensitivity and interaction of the two circulations is discussed more fully in Lu et al. (1998). The Weak Westerlies perturbation induces anomalies in ΔM_2 and ΔM_3. Similarly, the SVD3 experiment, and to a lesser extent the Zonal SVD3 experiment, have different ΔM_2 values than the Strong Trades case. This also seems to be largely related to changes in the IOC structure.

When the STC strength is modified by the Strong and Weak Trades perturbations, the equator responds not by changing the upwelling intensity w_1 over most of the upwelling region, but by changing the longitudinal extent of the upwelling region (Fig. 3c). This produces an upwelling anomaly (relative to the Base Run) over a relatively narrow region at the western edge of the Base

TABLE 1. Summary of steady numerical experiments: transport values of ΔM_i, W_{eq}, θ_{eq}, and T_{eq} for the Base Run, and for differences between test solutions and the Base Run (units are Sv and °C). Positive transport values represent either poleward or upward flows.

Quantity	Base Run	Strong Trades	Weak Trades	Weak Westerlies	SVD3	Avg SVD3
			Differences from Base Run			
ΔE	17.4	2.9	−2.9	0.0	2.8	2.8
ΔM_1	14.0	2.8	−2.6	−0.1	3.1	3.0
ΔM_2	−16.2	−2.1	1.9	0.4	−3.4	−2.9
ΔM_3	−7.7	−0.7	0.7	−0.3	0.2	−0.2
W_{eq}	25.2	3.2	−3.2	0.3	2.2	2.8
T_{eq}	25.7	−0.29	0.30	0.03	−0.21	−0.23
θ_{eq}	0.240	0.030	−0.030	0.002	0.020	0.024
			Fractional differences from Base Run			
ΔE	0.00	0.17	−0.17	0.00	0.16	0.16
ΔM_1	0.00	0.20	−0.19	−0.01	0.22	0.22
ΔM_2	0.00	0.13	−0.12	−0.02	0.21	0.18
ΔM_3	0.00	0.09	−0.09	0.04	−0.03	0.02
W_{eq}	0.00	0.13	−0.13	0.01	0.09	0.11
θ_{eq}	0.00	0.13	−0.13	0.01	0.08	0.10

Run upwelling (Fig. 4c). The temperature in most of the upwelling region is also about the same in the perturbation experiments, since the intensity of upwelling is the same. However, there is a temperature perturbation west of the upwelling (Fig. 4a), which is due to several factors. The most important is that the upwelling zone is shifted (westward, in the Strong Trades case), which offsets the curve of T_1 versus longitude (Figs. 3a,b). Because of the different net upwelling, T_1 at the western edge of the upwelling region is slightly different (in the Strong Trades case, stronger upwelling and cooler T_1). Finally, the westward flow is different (faster for Strong Trades), which changes the distance water flows before it is warmed to a given temperature by the restoring heat flux. The quantitative behavior of this decay is discussed more in section 5.

Equatorial T_2 perturbations are generally much smaller than perturbations in T_1 (Fig. 4b), except near the western boundary. The western anomalies are a consequence of the temperature gradient between northern-source and southern-source layer-2 water. In the western basin this temperature gradient follows the 18°C isotherm, which intersects the western boundary at the bifurcation point of the along-boundary flow (Fig. 2b). This bifurcation occurs at a slightly different point with different wind forcing and moves the temperature gradient along with it, changing the temperature near the boundary. These temperature anomalies are not the cause of the T_1 anomalies, because they are very weak in the upwelling region to the east, which is the only place where T_2 can influence T_1.

As expected, the Weak Westerlies perturbation does not induce much change in equatorial upwelling or temperature, since the STC transport is not modified significantly. Contrary to expectations, the SVD3 experiment has a smaller upwelling anomaly within 5° of the equator than the Strong Trades experiment, even with a larger ΔM_1 and ΔM_2. Since in steady state the upwelling equatorward of $\pm y_d$, W, must equal the total volume transport leaving the tropics in layer 1 (i.e., $W = M_1(y_d) - M_1(-y_d) + 5$ Sv, the last term resulting from the Indonesian Throughflow), the smaller equatorial upwelling implies different w_1 in the rest of the Tropics. The differences between the SVD3 and Strong Trades W_{eq} are partly accounted for by differences in coastal upwelling at the eastern boundary, and partly by differences in the strength of the tropical cell. The tropical cell consists of upwelled layer-1 water that returns to the thermocline just poleward of the Equatorial Undercurrent where h_2 thins to h_{2min} (see Lu et al. 1998).

Equatorial T_1 is generally cooler when there is stronger equatorial upwelling, warmer with weaker upwelling, and about the same as the Base Run in the Weak Westerlies case (Table 1). Not surprisingly, the SVD3 experiment, which has weaker equatorial upwelling than the Strong Trades experiment, also has a smaller T_1 anomaly.

The Weak Westerlies experiment, and the differences between the SVD3 and Strong Trades experiments, show that in terms of influence on equatorward thermocline flow, equatorial upwelling and SST, the subtropical wind (e.g., at 23°N) is more important than wind at higher latitudes, but that the higher latitude wind does have an influence, primarily through modifications to the IOC due to changes in layer-3 transport. Changes in the IOC are probably the cause of changes in the distribution of upwelling and downwelling within the tropics associated with the tropical cell. Comparison of the SVD3 and Zonal SVD3 cases show that there are also some differences between the effects of a simple wind perturbation and one that has zonal variations and a meridional component.

There is nothing special about the amplitude of the perturbation winds used here. Therefore it is useful to think of the perturbations in terms of fractional differences from the Base Run (second part of Table 1), so the fractional change in the forcing can be compared to fractional changes in key aspects of the response. We

TABLE 2. Oscillating response amplitude: M_1 and M_2 are at y_d, W_{eq} and T_{eq} are as in Table 1 (units are Sv and °C). Trades refers to wind perturbations centered at y_d, and Westerlies refers to wind perturbations centered at 39°N. Normalized amplitudes are divided by equilibrium response to steady wind perturbation at 100 yr (anomaly relative to Base Run).

	Trades		Westerlies	SVD3	
Variable	12 yr	24 yr	12 yr	12 yr	24 yr
			Amplitude of response		
M_1	3.20	2.77	0.14	3.52	2.74
M_2	0.87	1.48	0.34	1.17	1.41
W_{eq}	2.72	4.05	0.51	2.31	4.31
T_{eq}	0.25	0.39	0.05	0.20	0.40
			Amplitude normalized by corresponding steady response		
M_1	1.22	1.06	3.50	1.43	1.11
M_2	0.42	0.71	0.92	0.38	0.46
W_{eq}	0.85	1.26	1.70	1.04	1.93
T_{eq}	0.86	1.34	1.67	0.95	1.90

see that a 17% perturbation in the subtropical winds leads to about a 20% response in ΔM_1, a 13% response in ΔM_2 (22% for SVD3), and a 13% change in W_{eq} and θ_{eq} (weaker for SVD3, especially for θ_{eq}).

Liu and Philander (1995) also conduct steady wind perturbation experiments. They use a level model with a simplified geometry and forcing. Their ''half easterlies'' experiment is similar to our weak trades case but includes a weakening of the equatorial wind. Their half-subtropical case is similar to our weak westerlies case. They find only a small effect on tropical currents due to their ''subtropical'' wind, which is consistent with our negligible weak westerlies influence. In apparent contradiction to our results, their Table 1 shows the easterlies having only a small effect on the subtropical cell. However, they measure volume transport at 5°N; volume transport at a latitude corresponding to our y_d is more sensitive to the strength of the easterlies (see their Fig. 3).

Like us, Liu and Philander find that equatorial surface temperature is largely unaffected when the westerlies are reduced and is warmed by a reduction in upwelling when the easterlies are reduced. However, in contrast to our results, their perturbations (both easterlies and westerlies) significantly influence the thermocline temperature as well. A number of factors could cause this difference, including the differences in forcing and basin geometry and differences in vertical resolution and mixing between our $3\frac{1}{2}$-layer model and their level model. Even if our experiments underestimate the amount of wind-induced temperature change in the Equatorial Undercurrent and below, they clearly illustrate how surface temperature can be modified without deeper temperature changes.

4. Time evolution and response to periodic forcing

a. Model results for key parameters

The simplest extrapolation from the switched-on experiments would be if the oscillating wind produced a quasi-steady response; that is, if at some time the wind forcing has amplitude A, the ocean's response at that time is the same as the final response to a steady forcing of amplitude A. However, significant transient behavior in the ocean's response to the wind would complicate this behavior. In fact, as Table 2 shows, the amplitude of the oscillating response shows great variation for different variables and oscillation periods. Transport $M_1(y_d)$ is about the same as in the steady cases, while M_2 is considerably weaker. In this section, we compare $M_i(y_d)$ anomalies rather than ΔM_i anomalies, ignoring the small contributions at $-y_d$. Meanwhile, W_{eq} and T_{eq} are strongly dependent on the forcing period t_p, with the SVD3 winds producing an equatorial SST oscillation that ranges from about equal to the steady value to nearly twice as big.

Equatorial variations with the westerlies oscillation are smaller than with the other cases, but not as small as the steady experiments would suggest (Tables 2 and 1). Normalizing by the corresponding steady experiment values, the oscillation amplitudes of W_{eq} and T_{eq} are about twice as large as the oscillations in the trades case. Even with this enhancement, the T_{eq} oscillation is negligible in the westerlies case.

Some of this qualitative behavior can be guessed from the response of the ocean to a switched-on steady wind (Fig. 5). Transport $M_1(y_d)$ is dominated by $E(y_d)$, and so responds rather quickly to the wind (Fig. 5a). In contrast, $M_2(y_d)$ responds more slowly (Fig. 5a), presumably due to Rossby wave propagation. Transports W_{eq} and T_{eq} overshoot their final state (Fig. 5a), which may explain the fact that the oscillating response is actually stronger than the steady response. The overshoot behavior is interesting because it implies that there is some forcing period, which gives a maximum equatorial response. The T_{eq} overshoot follows from the upwelling overshoot. Looking at the Strong Trades experiment, we find that the net upwelling within 5° of the equator reaches a peak 30% higher than its final value at about year 8 of the experiment, while the net upwelling for the entire Tropics only overshoots by less than 10%. Thus much of the overshoot is caused by a strengthening

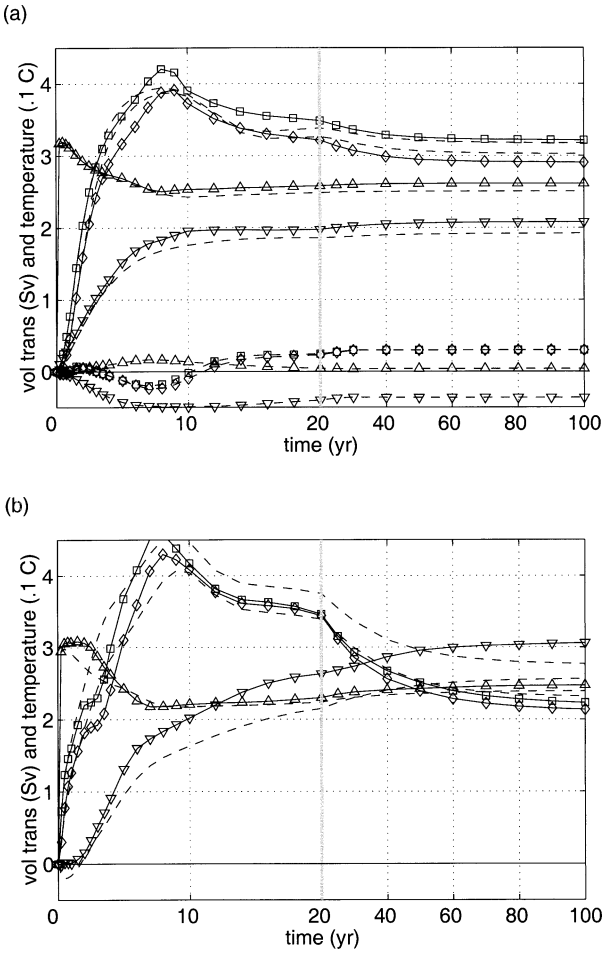

FIG. 5. Anomaly relative to Base Run as a function of time for $M_1(y_d)$ (triangle), $-M_2(y_d)$ (inverted triangle), W_{eq} (square), and $-T_{eq}$ (diamond). (Units are 1 Sv and 0.1°C.) Note that the time axis has two scales. (a) Strong Trades (solid lines), Weak Trades with reversed signs to facilitate comparison (dashed lines, large values), and Weak Westerlies (dashed lines, small values). (b) SVD3 (solid lines) and Zonal SVD3 (dashed lines).

and then weakening of the tropical cell over the first few decades after the wind perturbation starts.

b. *Predicting oscillating response from transient response*

In this subsection, we make a quantitative connection between the responses to switched-on and oscillating winds. We consider a wind perturbation with any of the spatial structures discussed above, but with the time-varying, nondimensional amplitude $a(t)$. Let Φ represent the resulting anomaly of any variable (M_2, W_{eq}, etc.), normalized by the final value induced by a steady wind perturbation.

The similar response of the ocean model to both negative and positive trade wind anomalies indicates that the system is roughly linear with respect to perturbations in the magnitude range we are studying. We therefore assume that the amplitude and response are related by a linear operator, L, so that

$$\Phi(t) = L[a(t)]; \tag{6}$$

note that we do not have an explicit expression for L. For the specific case of a switched-on wind, which can be written $a(t) = \theta(t)$ [where $\theta(t)$ is the stepfunction], $\Phi(t)$ is given by a function $S(t)$, such as the normalized versions of the curves shown in Fig. 5.

The goal is to use our knowledge of $S(t)$ to calculate $\Phi(t)$ for any $a(t)$. To do this, we use the identity

$$\begin{aligned} a(t) &= \int_{-\infty}^{+\infty} a(t')\delta(t' - t)\, dt' \\ &= \int_{-\infty}^{+\infty} a_{t'}\, \theta(t - t')\, dt', \end{aligned} \tag{7}$$

where $\delta(t)$ is a delta function. Substituting (7) into (6) and remembering that L operates on t but not t', we obtain

$$\Phi(t) = \int_{-\infty}^{+\infty} a_{t'}(t') L\,[\theta(t - t')]\, dt'. \tag{8}$$

If we substitute $S(t) = L[\theta(t)]$ into (8), then (8) becomes

$$\Phi(t) = \int_{0}^{t} a_{t'}(t') S(t - t')\, dt'. \tag{9}$$

Equation (9) expresses the idea that continuously changing forcing is the superposition of a series of infinitesimal increments in forcing, each of which causes a response proportional to S to be added to the response to previous forcing increments.

Since the forcing we are interested in is sinusoidal, we now restrict $a(t)$ to the form (4). Equation (9) can then be written

$$\begin{aligned} \Phi(t) = \omega a_0 \Bigg[&\cos(\omega t) \int_0^t S(r)\, \sin(\omega r)\, dr \\ &+ \sin(\omega t) \int_0^t S(r)\, \cos(\omega r)\, dr \Bigg], \end{aligned} \tag{10}$$

where $\omega = 2\pi/t_p$. To take advantage of the assumption that $S(t) \to 1$ for t sufficiently large, it is convenient to define the integrals

$$I_1 = \omega \int_0^t (S(r) - 1)\, \cos(\omega r)\, dr \tag{11a}$$

$$I_2 = \omega \int_0^t (S(r) - 1)\, \sin(\omega r)\, dr, \tag{11b}$$

which are both independent of t for large t. Then (10) can be written

$$\frac{\Phi(t)}{a_0} = D \sin\left(2\pi \frac{t - \psi}{t_p}\right), \tag{12}$$

where the amplitude is

$$D = \sqrt{I_1^2 + (1 + I_2)^2} \tag{13}$$

and the phase shift is

$$\psi = -\frac{1}{\omega} \arctan\left(\frac{I_1}{1 + I_2}\right). \tag{14}$$

The utility of (12) (and the accompanying definitions) is that given the transient behavior from a single numerical experiment, $S(t)$, we can predict the response to forcing over a wide range of oscillation periods without conducting any additional numerical experiments.

We test the transform idea by comparing to the numerical results. If we let Φ be $M_2(y_d)$, the response to the initiation experiment (Weak Trades) is approximated by

$$S(t) = 1 - e^{-t/t_i}, \tag{15}$$

where $t_i = 4.3$ yr. In this case, it is easy to integrate (11) analytically, and we obtain an amplitude of

$$D = \frac{1}{\sqrt{1 + (2\pi t_i/t_p)^2}}. \tag{16}$$

For forcing periods of 12 and 24 yr, D is predicted to be 0.41 and 0.66, respectively, which are close to the corresponding values obtained from the numerical experiments (0.42 and 0.71 in Table 2). Thus, we see that the weak amplitude of $M_2(y_d)$ in the oscillatory solution follows directly from the slowness of the tropical response.

The phase shift ψ for this case also has a simple expression,

$$\psi = \omega \arctan(2\pi t_i/t_p). \tag{17}$$

Note that $\psi = t_i$ for sufficiently large values of t_p, whereas it is approximately $t_p/4$ for small t_p. The phase shift ψ is predicted to be 2.2 yr for $t_p = 12$ yr and 3.2 yr for $t_p = 24$ yr, in good agreement with the numerical experiment values of 2.3 and 2.9 yr.

Other $S(t)$ curves are not as easily approximated with an analytic expression. However, the amplitude D of the response to the oscillating wind of each variable can be predicted from $S(t)$ of the variable by numerically evaluating the integrals in (10) when $a(t)$ is given by (4). Table 2 compares the actual response for the four quantities, $M_1(y_d)$, $M_2(y_d)$, W_{eq} and T_{eq}, for each of four wind perturbations (Weak and Strong Trades, SVD3, and Weak Westerlies) and for the 12- and 24-yr periods. The responses to the oscillating winds cover a substantial range, from about 0.5 to 4, and nearly all predictions are within 10% of the corresponding values from the numerical experiments (one is within 14%).

Using the switched-on experiments to predict the response to oscillating forcing allows us to calculate the response (both amplitude and phase lag) to a wide range of forcing periods (see Fig. 6 for the trades perturbation). For the physical quantities we examine, $D(t_p)$ is similar to the corresponding $S(t)$ in the switched-on experiment (Figs. 5 and 6a). However, the timescales for characteristic features in $D(t_p)$ are longer than for the corresponding $S(t)$. For example, for the exponential case discussed above, it can be shown analytically that for small t and t_p), $dD/dt_p = dS/d(2\pi t)$. This explains why details of the first few years of a variable's response to switched-on winds can influence the periodic response to decadal oscillations.

As with D, the predictions for phase lag $\psi(t_p)$ are fairly close to values from the numerical experiments (Fig. 6b). The shape of the curves are very different for different variables. For $M_2(y_d)$, the behavior is similar to the analytic prediction, with ψ increasing strongly with t_p for small t_p and reaching an asymptote of around 5 yr for large t_p. The phase lag for $M_1(y_d)$ is generally

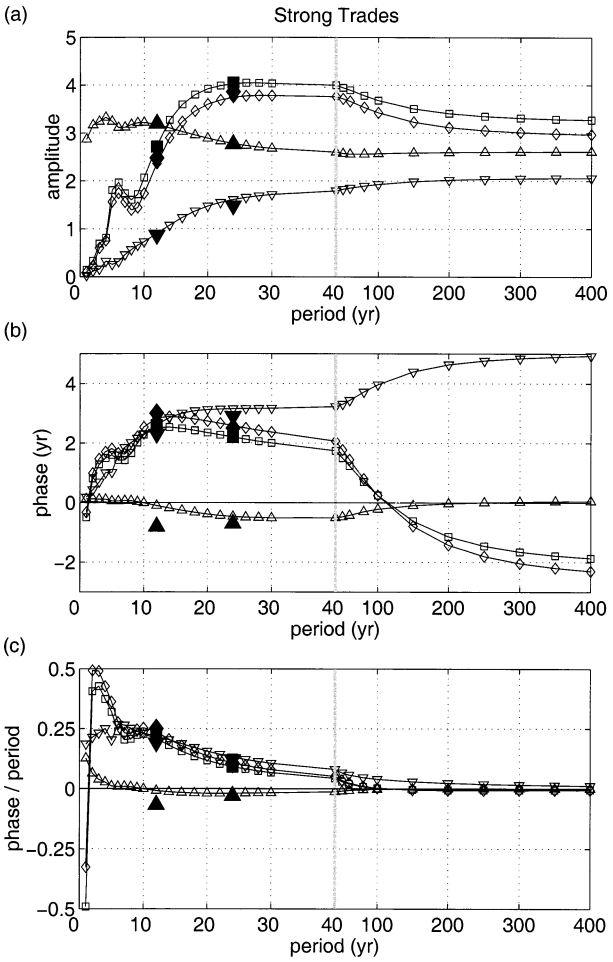

FIG. 6. Response to oscillating forcing (Strong Trades case) as a function of forcing period t_p for theory (open symbols) and numerical experiments (filled symbols) for $M_1(y_d)$ (triangle), $M_2(y_d)$ (inverted triangle), W_{eq} (square), T_{eq} (diamond). (a) Amplitude D. (b) Phase lag, ψ. (c) Normalized phase lag, ψ/t_p.

much smaller, as we would expect from the fact that $S(t)$ does not change much over time. That $S(t)$ decreases with time produces a negative phase lag. The W_{eq} and T_{eq} lags have features of both M_1 and M_2 lags. For small t_p, they are like $M_2(y_d)$, responding to the strong initial change in $S(t)$. For larger t_p they go to a negative asymptote, responding to the decrease in $S(t)$ for large t. Thus, for forcing periods of up to about a decade, the equatorial response slightly lags $M_2(y_d)$, while for longer periods, the equatorial response leads by increasing amounts.

It may seem counterintuitive that the phase lag is not greatest for small t_p, since one expects the system to be closer to the equilibrium solution for increasing t_p. If we plot phase lag normalized by t_p (Fig. 6c), however, we see that the longest phase lags (as a fraction of the forcing period) do occur for short periods. For all variables, the normalized lag goes to zero for large t_p.

The different temporal behaviors of $M_1(y_d)$, $M_2(y_d)$, and W_{eq} (Figs. 5 and 6) show that we can not think of the STC as a simple current loop in which all parts of the loop speed up or slow down in unison. Instead, an abrupt change in the wind brings a fast response in the poleward surface flow, a slow response in the equatorward thermocline flow, and a more complicated response in equatorial upwelling (which directly controls equatorial SST). For periodic forcing, the response strength depends on the period, but both $M_1(y_d)$ and W_{eq} generally have stronger responses (relative to their steady values) than $M_2(y_d)$. In the case of W_{eq}, the stronger response at decadal periods is related both to the overshoot and to the steeper slope for the first 5 yr or so of its $S(t)$. There are also differences between the different parts of the STC in the final steady response to perturbations. Together these factors cause the amplitude of W_{eq} to be more than twice as big as the amplitude of $M_2(y_d)$ for oscillations on decadal time scales, with W_{eq} variations leading $M_2(y_d)$ variations. If the real ocean behaves the same way, observations of decadal changes in $M_2(y_d)$ could seriously underestimate the importance of these changes to the equatorial upwelling and SST unless the differences in response are taken into account.

c. Response to westerlies and SVD3 perturbations

The Weak Westerlies switched-on experiment has a more complicated evolution than the Trades experiments (Fig. 5a). Just as in the steady case, the transient response is much weaker than the response to perturbations in the trade winds. The SVD3 experiment's evolution has small differences from the Strong Trades experiment (Fig. 5b) due to the differences in the zonal average zonal wind (principally at high latitudes) and to the more complicated structure of the wind. To separate these two influences, we look at the Zonal SVD3 experiment evolution (Fig. 5b). In both SVD3 experiments, $M_2(y_d)$ takes longer to start growing, perhaps

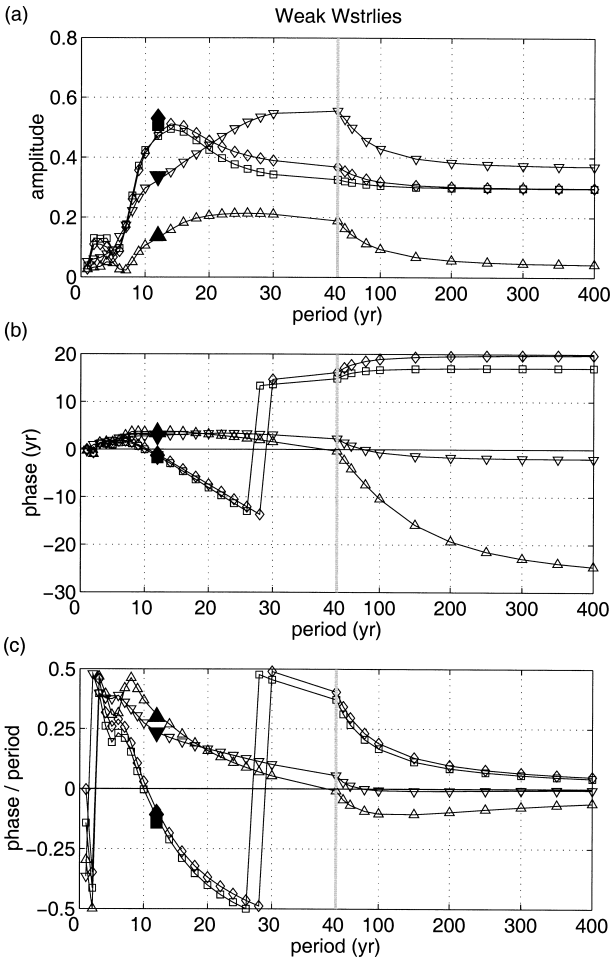

FIG. 7. As in Fig. 6 but for Weak Westerlies perturbations.

because of the contribution of the high latitude winds. On the other hand, W_{eq} grows *faster* than the Strong Trades case for both SVD3 experiments, but then decreases by a larger amount than the Strong Trades from the peak value at about 8 yr.

As in the last section, we use the switched-on behavior to calculate the amplitude and phase lag of the response to periodic forcing. The Weak Westerlies response has a relatively small amplitude for all t_p (Fig. 7a). All four variables have very small amplitudes for small t_p and a maximum amplitude at 10–40 yr. The phase lags tend to be relatively long (up to nearly 20 yr; see Fig. 7b); the discontinuity in the plots is due to the convention of switching from a negative value to a positive value at $\psi = 0.5t_p$ (Fig. 7c). The responses in the SVD3 experiment (Fig. 8) are broadly similar to the Strong Trades responses (Fig. 6), though there are some significant differences. The SVD3 W_{eq} and T_{eq} amplitudes have a more complicated shape for $t_p < 15$ yr due to relatively subtle differences in the small-t behavior in the corresponding switched-on response (Fig. 5). The long-period phase lags are much longer than the Strong

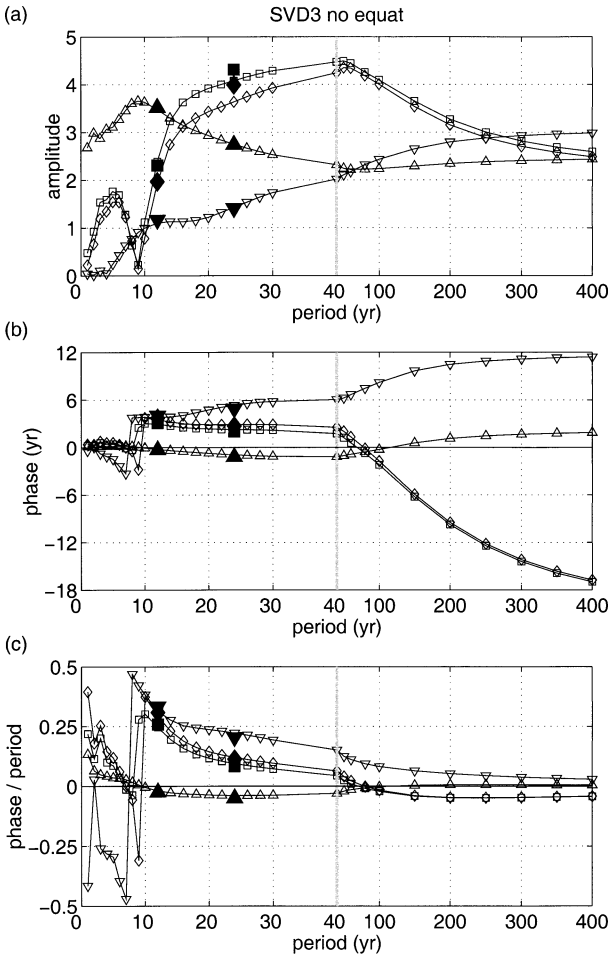

FIG. 8. As in Fig. 6 but for SVD3 perturbations.

Trades case, and ψ for the equatorial variables also show an abrupt change at about $t_p = 10$ yr.

To summarize, these experiments show that the response to an oscillating subtropical–midlatitude wind perturbation is dominated by the zonal-mean perturbation to the trade winds, but that the midlatitude component and more complicated spatial structure does have some influence, for instance on the phase lag at decadal and longer forcing periods.

5. Equatorial temperature profile

Here, we again consider steady solutions, investigating how the distribution of equatorial temperature depends on forcing and other parameters. We assume that the equatorial surface flow is zonal (westward) along the equator, and fed by upwelling from layer 2, and ignore horizontal diffusion terms. All these assumptions appear to be true in the numerical experiments. With these assumptions, equatorial T_1 (designated here as a function only of zonal distance x) is given by

$$U_1 dT_1(x)/dx = \lambda H_q(T_* - T_1) + w_1(T_2 - T_1), \quad (18)$$

where $U_1 \equiv h_1 u_1$, w_1 is across-interface (entrainment) velocity in the upwelling region, λ is the recipricol of a time constant, and H_q is a constant depth scale. For simplicity, we take T_* and T_2 to be constants, which is a good approximation in our numerical solutions. We nondimensionalize variables with $x \sim L_1$ (the longitudinal extent of the upwelling region), $w_1 \sim W$, $U_1 \sim U_0 = WL_1$, and $T_1 \sim T_* - T_2$. Then, (18) becomes

$$U_1 \theta_x = -\eta\theta + w_1(1 - \theta), \quad (19)$$

where U_1, x and w_1 are now nondimensional quantities, θ is given by (5), and

$$\eta = \frac{\lambda H_q}{W} \quad (20)$$

measures the relative strengths of (dimensional) upwelling and restoring.

To solve (19), we need to specify U_1 and w_1 as functions of x. We assume that $w_1 = 0$ west of some longitude, which we designate $x = 0$. We examine the upwelling region ($x > 0$) first. For our simplest case, we assume further that $w_1 = 1$ for $x > 0$, and, ignoring v_y in the continuity equation, it follows that $U_1 = -(1 - x)$. With these assumptions, (19) can be written

$$(x - 1)\theta_x = -\eta\theta + 1 - \theta. \quad (21)$$

Solving first for the homogeneous solution via separation of variables, and using this to find the complete solution, yields

$$\theta = \left[\frac{(1 - x)^{1+\eta}}{1 + \eta} + c\right](1 - x)^{-(1+\eta)}, \quad (22)$$

where c is a constant. Unless we set $c \neq 0$, however, (22) implies the physically unreasonable condition that $\theta \to \infty$ as $x \to 1$. Therefore, we set $c = 0$, and (22) reduces to

$$\theta = \frac{1}{1 + \eta}. \quad (23)$$

While (23) predicts $T_1(x)$ to be uniform in the upwelling region, the numerical experiment (Figs. 3a,b) does show some variation with longitude. This is because w_1 is not uniform (Fig. 3c) contrary to the assumption here. However, we can still use (23) to roughly estimate the magnitude of θ.

For the Base Run, $\lambda = 1/180$ days, $H_q = 100$ m, and the net upwelling averaged over the 60° of longitude where w_1 is significant (within 0.5° of the equator) gives $W = 370$ m yr^{-1}. Given the meridional Ekman transport associated with the STCs, this value can be approximately obtained from first principles if the length and width of the upwelling region can be calculated, though the tropical recirculation and interocean circulation somewhat modify this value. Here we have calculated w_1 from the numerical results. From definition (20), the values above give $\eta = 0.55$, so (23) predicts $\theta = 0.65$. As Fig. 3b shows, the actual value of θ in the upwelling

region ranges from 0.26 to 0.67, with an average value of 0.49.

The previous analysis gives a broadly accurate estimate of the magnitude of the equatorial temperature minimum induced by the equatorial upwelling. We now make a more precise estimate of θ in the upwelling region, using somewhat more detailed information from the numerical experiment. The main motivation is to see whether the ordinary differential equation representing the balance of upwelling, zonal advection, and atmospheric restoring is indeed a valid approximation to the full temperature equation. We set

$$w_1(x) = 1 + \Omega(1 - 2x), \tag{24}$$

rather than a constant. In the uniform-w_1 solution discussed above, forcing θ to be finite at $x = 1$ is equivalent to removing the $U\theta_x$ term in the equation, so the exact form of $U(x)$ is irrelevant to the solution. With w not uniform, this is no longer the case. In the Base Run, there is substantial meridional flow away from the equator, so that $U_1(x)$ is much less than the integral of w_1 assumed above. For simplicity, we take

$$U_1(x) = -\alpha(1 - x), \tag{25}$$

which is a good approximation to the actual variation for $\alpha = 1/3$.

Using the methods described above and the condition that θ must be finite everywhere, we obtain

$$\theta(x) = -\theta_H(x) \int_x^1 \frac{w_1}{U_1 \theta_H}\, dx, \tag{26}$$

where

$$\theta_H(x) = \exp\left(-\int \frac{\eta + w_1}{U_1}\, dx\right). \tag{27}$$

For the specific w_1 and U_1 defined above, the solution to (27) is

$$\theta(r) = \frac{e^{-2\Omega r/a}}{cr^p} \int_0^r \left(2\Omega + \frac{1 - \Omega}{r}\right) r^p e^{2\Omega r/a}\, dr, \tag{28}$$

where for convenience we have defined $r = 1 - x$ and $p = (1 + \eta - \Omega)/a$. Unfortunately, there is not an analytic solution to this integral. However, since $e^{2\Omega r/a} \to 1$ as $r \to 0$, the eastern limit of θ can be evaluated and is

$$\theta_E = \frac{1}{1 + \eta/(1 - \Omega)}. \tag{29}$$

Not surprisingly, the eastern boundary value does not depend on α, the magnitude of U_1.

To obtain a solution for the entire x range, we expand the exponential in the integral in a power series, each term of which can be integrated analytically, and then evaluate the resulting series numerically. Retaining the first 20 terms gives an approximation that solves (19) with an error of less than 0.001θ. We plotted the solution

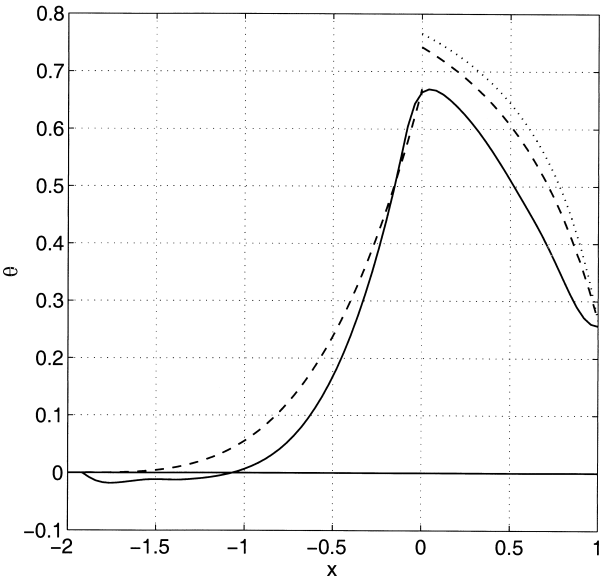

FIG. 9. Base Run $\theta(x)$ along the equator (as in Fig. 3) as a function of nondimensional $x = (x - 100°)/50°$ (solid), along with prediction for the western no-upwelling region from (32) and for the eastern upwelling region from (28) (both dashed), and the $U_1 = 0$ solution shown in (30) (dotted).

(not shown) for η ranging from 0.25 to 4; for Ω of 0, 0.5, 0.9, and 1; and for α of 1/3 and 1. Variable $\theta(x)$ increases monotonically from east to west with roughly the same profile for all cases, the profiles becoming more uniform as Ω approaches 0 ($\Omega = 0$ is the uniform-w, uniform-θ case). Using the parameters appropriate for the base run ($\eta = 0.55$, $\Omega = 0.8$, $a = 1/3$), (28) predicts $\theta(x)$, which is in good agreement with the base run temperature in the equatorial upwelling region (Fig. 9, $x > 0$ range of the graph), with a predicted peak value about 10% higher than the model and the eastern boundary prediction even closer.

It is interesting that the solution does not change much when α is changed from 1/3 to 1. This lack indicates that the temperature profile in the upwelling region is primarily established by the balance between the upwelling rate and restoring heat flux, and that horizontal advection is not so important. If we take the extreme case of simply ignoring the U_1T_x term in (19), the equation ceases to be a differential equation and is solved by

$$\theta(x) = \frac{w_1}{w_1 + \eta}. \tag{30}$$

Figure 9 includes this function (calculated with the parameter values listed above) to show that simply balancing upwelling with atmospheric forcing gives a fairly good approximation to the actual temperature profile in this region.

In the western ocean ($w_1 = 0$ and $x < 0$), advection determines how far to the west the temperature anomaly persists. Roughly speaking, the larger the speed of the surface current relative to the restoring timescale, the

larger is the region that is anomalously cool. The zonal volume transport must decrease as we travel westward in order to feed the meridional flow leaving the equator. We assume the simplest meridional velocity structure—hv_1 independent of x—which in fact gives a good approximation to the actual Base Run nondimensional U_1 profile, $U_1 = -(1 + \epsilon x)$. Here $\epsilon = L_1/L_2$, and the western boundary is at $x = -L_2$. In this case, (19) becomes

$$(1 + \epsilon x)\theta_x = \eta\theta, \tag{31}$$

which is solved by

$$\theta = \theta_0(1 + \epsilon x)^{\eta/\epsilon}, \tag{32}$$

where θ_0 is the value of θ at $x = 0$. Taking θ_0 from the numerical results, we plot the theoretical θ in the $w_1 = 0$ region along with the model values over the whole domain (Fig. 9). The predicted decay scale is roughly the correct size, though a little longer than in the numerical experiment.

These results are consistent with a similar box model for equatorial temperature by Sun and Liu (1996). Our results extend Sun and Liu's work by making a more direct quantitative comparison between theory and numerical result, looking at zonal variations within the two equatorial regions (upwelling and nonupwelling), and allowing upwelling strength to have a remotely forced component.

While simple theory gives a good approximation to the model's equatorial temperature, there are significant discrepancies between the model's SST and that of the real ocean. In particular, the eastern equator is too cold compared to the west, and the zonal temperature gradient is too concentrated in the eastern region. Some limitations of our numerical model are the simplified restoring temperature used, the uniform value of λ (a measure of the sensitivity of surface heat flux to SST departures from the restoring temperature), and the fact that the strongest equatorial upwelling occurs farther from the eastern boundary than in the real world. This last discrepancy may be related to the simple vertical structure of the model, an issue we hope to address in the future. The broader question, which is beyond the scope of this paper, is understanding the longitude–depth structure of the real ocean's vertically continuous equatorial thermocline.

6. Conclusions

In this paper we have built on previous studies of the steady circulation to understand the response of the equatorial Pacific Ocean to subtropical wind variability with periods of years to decades. Our immediate motivation is the ocean–atmosphere oscillation described in Kleeman et al. (1999), but tropical variability due to midlatitude and subtropical forcing has also attracted much other attention recently (Deser et al. 1996; Gu and Philander 1997; Lysne et al. 1997; Zhang et al. 1998). There are two broad thrusts to this paper: One is to couple our picture of the thermocline and upper ocean circulation to a simple model of the thermodynamics in order to quantify the effect of the mean circulation on the surface layer equatorial temperature. The other is to compare solutions forced by oscillating wind perturbations to those forced by switched-on versions of the same perturbations. Throughout, we conduct numerical experiments with a fully nonlinear, $3\frac{1}{2}$-layer model of the Pacific Ocean and use simple analytic models to gain insight into the model's behavior.

The equatorial temperature in our steady Base Run with climatological forcing is well-approximated by balancing surface forcing, zonal advection, and vertical advection. In our experiments, the equatorial surface layer falls into two dynamically distinct regimes. In the eastern region, where there is strong across-isopycnal upwelling, the temperature is dominated by the balance between upwelling and atmospheric forcing; model SST is relatively insensitive to the proportion of upwelled water that flows westward and the proportion that flows directly away from the equator. In the western two thirds of the equator, there is no across-isopycnal flow, so zonal advection becomes crucial in determining the distance over which the temperature is restored to a reference temperature. In our model, the reference temperature is simply observed SST in the western Pacific, but in the real world the reference temperature should include radiative effects as described by Haney (1971).

The circulation's equilibrium response to steady subtropical and midlatitude wind perturbations is broadly consistent with the results of Lu et al. (1998), which links the surface Ekman transport to the subtropical cell, interocean circulation, and tropical cells. Key indices of the system are the surface and thermocline flow between the tropics and subtropics, equatorial upwelling, and equatorial temperature anomaly. Changes in tropical circulation and SST are most strongly influenced by the subtropical cell, with $O(10\%)$ changes in the subtropical wind causing $O(10\%)$ changes in these indices. A somewhat more idealized study by Liu and Philander (1995) showed similar surface layer equatorial temperature response to steady wind perturbations but some differences in equatorial thermocline temperature. The wind perturbation pattern associated with decadal variability in KMK (referred to as SVD3) is strong in subtropical and midlatitude bands. For the wind anomaly strength used here (and for values likely to occur on decadal scales in the real ocean), the system appears to be in a linear regime, so that it is reasonable to sum the responses due to wind contributions in different geographical areas.

When the wind perturbations oscillate, the magnitude of the response for 12- and 24-yr periods differ from each other and from the steady response. Because the response is approximately linear, it is straightforward to derive the oscillatory behavior from the transient response to a switched-on perturbation. This allows us to predict the response to all forcing periods on the basis

of a single numerical experiment, and makes it easier to interpret the differences between the steady and oscillatory response.

A striking feature of the response to a 12-yr oscillating trade winds perturbation is that $M_2(y_d)$, the meridional transport of thermocline water across the edge of the northern Tropics, is less than half as strong as the steady value, while $M_1(y_d)$, the surface transport, is somewhat stronger than the steady value. The transient response to a switched-on wind perturbation shows that $M_2(y_d)$, which is dominated by geostrophic flow, takes nearly a decade to get close to its final value, while $M_1(y_d)$, dominated by Ekman transport, responds immediately. This difference implies that in the real ocean, changes in the thermocline flow will underpredict the strength of equatorial changes driven from the subtropics. Similarly, $M_2(y_d)$ anomalies tend to lag both the wind and the $M_1(y_d)$ anomalies.

Amplitudes of anomalies in oscillating equatorial upwelling W_{eq} and equatorial surface temperature T_{eq} can be smaller or larger than the steady value, depending on the period, but the W_{eq} anomalies are generally larger than M_2 anomalies. The larger values are due to the maximum in $W_{eq}(t)$ [also occuring in $T_{eq}(t)$] that occurs about 8 years after the wind perturbation is imposed. This overshoot is linked to a decadal-scale transient in the tropical cell, which is confined to about 10° either side of the equator. The overshoot also makes the phase lag for the oscillating case decrease with forcing period for multidecadal periods. Thus, $M_2(y_d)$ also lags W_{eq} and T_{eq}.

As expected, westerly wind perturbations and more complicated wind structure have a smaller effect than the trades perturbations on the subtropical and equatorial signals. Therefore, decadal wind oscillations such as SVD3 (see above) produce a response that is similar to that of a simple trades perturbation alone, but with some quantitative differences in both magnitude and phase lag.

Acknowledgments. Part of this research was carried out while Jay McCreary was a faculty member at the Nova Southeastern University Oceanographic Center and while Richard Kleeman was at the Bureau of Meteorology Research Centre. Programming assistance was provided by Elena Boguslavsky, who also helped evaluate the integral in section 5, and by Kevin Kohler. We thank Zhengyu Liu and an anonymous reviewer for thoughtful comments. This research was supported by the GOALS program through NOAA Grant NA76GP0353, and by the Frontier Research System for Global Change through its sponsorship of the International Pacific Research Center (IPRC).

REFERENCES

Deser, C., M. A. Alexander, and M. S. Timlin, 1996: Upper-ocean thermal variations in the North Pacific during 1970–1991. *J. Climate,* **9,** 1840–1855.

Gu, D.-F., and S. G. H. Philander, 1997: A theory for decadal climate fluctuations. *Science,* **275,** 805–807.

Haney, R. L., 1971: Surface thermal boundary condition for ocean circulation models. *J. Phys. Oceanogr.,* **1,** 241–248.

Harrison, D. E., 1989: On climatological monthly mean wind stress and wind stress curl fields over the world ocean. *J. Climate,* **2,** 57–70.

Hellerman, S., and M. Rosenstein, 1983: Normal monthly wind stress over the world ocean with error estimates. *J. Phys. Oceanogr.,* **13,** 1093–1104.

Inui, T., K. Takeuchi, and K. Hanawa, 1999: A numerical investigation of the subduction process in response to an abrupt intensification of the westerlies. *J. Phys. Oceanogr.,* **29,** 1993–2015.

Johnson, G. C., 2001: The Pacific Ocean subtropical cell surface limb. *Geophys. Res. Lett.,* **28,** 1771–1774.

Kleeman, R., J. P. McCreary, and B. A. Klinger, 1999: A mechanism for generating ENSO decadal variability. *Geophys. Res. Lett.,* **26,** 1743–1746.

Levitus, S., and T. P. Boyer, 1994: *Temperature.* Vol. 4, *World Ocean Atlas 1994,* NOAA Atlas NESDIS 4, 117 pp.

Liu, Z., 1994: A simple model of the mass exchange between the subtropical and tropical ocean. *J. Phys. Oceanogr.,* **24,** 1153–1165.

——, 1999: Forced planetary wave response in a thermocline gyre. *J. Phys. Oceanogr.,* **29,** 1036–1055.

——, and S. G. H. Philander, 1995: How different wind stress patterns affect the tropical-subtropical circulations of the upper ocean. *J. Phys. Oceanogr.,* **25,** 449–462.

——, ——, and R. C. Pacanowski, 1994: A GCM study of tropical–subtropical upper-ocean water exchange. *J. Phys. Oceanogr.,* **24,** 2606–2623.

Lu, P., and J. P. McCreary, 1995: Influence of the ITCZ on the flow of thermocline water from the subtropical to the equatorial Pacific Ocean. *J. Phys. Oceanogr.,* **25,** 3076–3088.

——, ——, and B. A. Klinger, 1998: A numerical investigation of the source waters of the Pacific Equatorial Undercurrent. *J. Phys. Oceanogr.,* **28,** 62–84.

Lysne, J., P. Chang, and B. Giese, 1997: Impact of the extratropical Pacific on equatorial variability. *Geophys. Res. Lett.,* **24,** 2589–2592.

McCreary, J., and P. Lu, 1994: Interaction between the subtropical and equatorial ocean circulations: The subtropical cell. *J. Phys. Oceanogr.,* **24,** 466–497.

Rothstein, L. M., R.-H. Zhang, A. J. Busalacchi, and D. Chen, 1998: A numerical simulation of the mean water pathways in the subtropical and tropical Pacific Ocean. *J. Phys. Oceanogr.,* **28,** 322–343.

Sun, D.-Z., and Z. Liu, 1996: Dynamic ocean–atmosphere coupling: A thermostat for the Tropics. *Nature,* **272,** 1148–1150.

Zhang, R.-H., L. M. Rothstein, and A. J. Busalacchi, 1998: Origin of upper-ocean warming and El Niño change on decadal scales in the tropical Pacific Ocean. *Nature,* **391,** 879–882.